Experimental Characterization Of Compaction Behavior Of Roving Based Reinforcements

Pouchias, A.; Yuksel, O.; Caglar, B.

Publication date
2024

Document Version
Final published version

Published in
Proceedings of the 21st European Conference on Composite Materials

Citation (APA)
Pouchias, A., Yuksel, O., & Caglar, B. (2024). Experimental Characterization Of Compaction Behavior Of Roving Based Reinforcements. In C. Binetury, & F. Jacquemin (Eds.), *Proceedings of the 21st European Conference on Composite Materials: Volume 5 - Manufacturing* (Vol. 5, pp. 627-633). The European Society for Composite Materials (ESCM) and the Ecole Centrale de Nantes..

EXPERIMENTAL CHARACTERIZATION OF COMPACTION BEHAVIOR OF ROVING BASED REINFORCEMENTS

A. Pouchias[1], O. Yuksel[1] and B.Caglar[1,*]

[1]Department of Aerospace Structures and Materials, Faculty of Aerospace Engineering, Delft University of Technology, the Netherlands

[*]Corresponding author (b.caglar@tudelft.nl)

Keywords: compaction, continuous processes, material characterization, mechanical testing

Abstract

This paper presents an experimental investigation into the compaction behavior of roving-based unidirectional (UD) reinforcements. Understanding the complex dynamics of roving compaction is essential for ensuring the quality in composite manufacturing processes and in return to reach optimal performance. In continuous manufacturing processes like pultrusion or tape manufacturing, achieving proper compaction of rovings is crucial for reaching high fiber volume fractions and consequently, the desired mechanical properties in the final composite profile. However, high compaction in rovings poses challenges, particularly during the impregnation phase, where pressure buildup can occur, potentially leading to the formation of undesirable voids or to excessive forces on fiber, causing fuzz accumulation. Balancing the need for high compaction with the risk of defects is thus a delicate exercise, critical for ensuring the quality and integrity of the final product. Through experimental characterization and analysis, this work examines the influence of various factors to the compressibility of rovings, including the application of tension and different configurations in dry conditions. This study aims to provide valuable insights into characterizing the compaction behavior of roving-based reinforcements and the effect of applied tension, thereby advancing the state-of-the-art in continuous composite manufacturing processes.

1. Introduction

Composite materials have gained significant attention in various industries due to their exceptional properties, including high strength-to-weight ratio and corrosion resistance. Roving-based reinforcements, consisting of continuous fibers bundled together, are widely used in composite manufacturing to impart strength and stiffness to the final product [1]. Many fiber-reinforced composites manufacturing processes involve the through-thickness compaction of the fiber network. This can lead to fiber movement depending on the sequence of the manufacturing phases [2]. In case of a shear induced displacement of the fibers and their rovings, they are nested and densely packed in areas towards the center of a profile which can alter their orientation, fiber volume fraction, and eventually the permeability [3-6]. Notably, the compaction characteristics of rovings during the pultrusion process can affect both the processing parameters and mechanical properties of the final part [7, 8]. Alterations of the volume fraction during compression result in permeability variations directly affecting the liquid resin impregnation. Consequently, achieving uniform compaction of roving-based reinforcements during the manufacturing processes poses significant challenges. By comprehensively characterizing compaction behavior of roving based reinforcements, designers and manufacturers can identify optimal processing parameters and strategies to minimize defects such as voids, resin-rich areas, and fiber misalignment.

In this study, a new experimental testing approach is demonstrated for characterizing the compaction of roving-based reinforcements. Specifically, the compaction behavior of rovings under different tensions and various roving configurations, in the absence of transverse constraints and in dry conditions, was examined. Main motivation is to gain an understanding of the link between the compressibility changes and the applied axial tension which is present in some continuous process like pultrusion [9] or tape manufacturing. The test procedure and equipment instrumentation followed the guidelines of the recent benchmark exercise [2], with additional tools for the placement and tensioning of the rovings. Hence, the aim of this work is to analyze the effects of applied tension and different roving configurations on the compaction behavior. The experimental campaign, results, and observations are discussed in the following sections.

2. Methodology

2.1. Experimental Design

The experimental setup consists of a modular aluminum frame, two solid stiff compaction circular plates, and a Universal Testing Machine (UTM) as outlined in Figure 1. The aluminum frame was designed and manufactured to adjust the location of the roving holders based on the number of rovings and the height of the UTM. Additionally, 3D printed rollers were chosen as roving holders instead of guides to allow for the rotation of the mounting and to minimize friction when tension is applied.

It was decided to employ three tension levels and three different configurations of carbon fiber rovings under dry conditions. Tension was applied by affixing weights to one end of each roving and securing the other end to the frame using clamps. In this manuscript, the tension levels are referred to as follows: no tension (T_0), low tension (T_1), which equated to 1 N and was achieved using 100g weights, and high tension (T_2), equivalent to 5 N, accomplished with 500g weights. These values are referred to the tension and weights applied to each roving individually. Also, roving configurations include one row of rovings (C_4), quadratic (C_9) and hexagonal (C_{11}) distributions as visualized in Figure 1.

The material used in this study is the carbon fiber filament T700SC-12K-60E, supplied by TORAY [10]. Prior to roving placement, the rollers were fixed in their locations, allowing only rotation. Rovings were then carefully placed on top of each holder without twisting and secured at one end. For the zero-tension case, the other end remained free, while for the tension cases, weights were hung from each roving. Each case study was repeated three times with a fresh specimen.

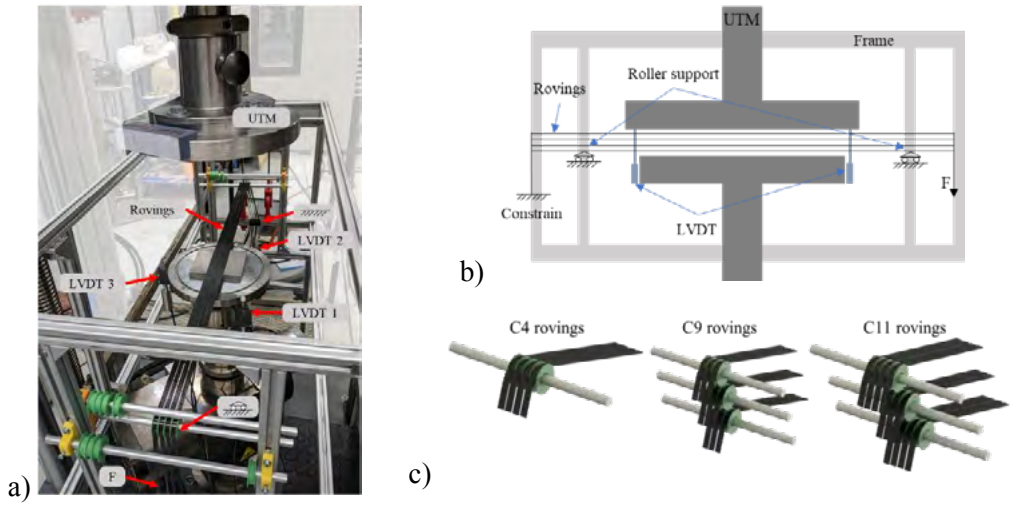

Figure 1. a) Picture of the experiment for 4-rovings configuration, b) Schematic diagram of the experimental setup, c) Representation of the roving configurations.

2.2. Testing method

Prior to conducting the experiments, compliance runs and Linear Variable Differential Transformer (LVDT) calibration tests were performed to mitigate the influence of the testing machine and enhance result accuracy. All samples underwent compression at a cross-head speed of 1 mm/min until reaching the maximum force limit of 3000 N, which was sustained for 180 seconds to ensure stability. Subsequently, the top plate was separated at the same speed (1 mm/min). This cycle was repeated three times for each test. An example of the measured force and tool separation during the testing procedure is given in Figure 2a.

The tool separation, measured with the UTM during the tests, was later adjusted using the compliance curves. The measured tool separation using the LVDTs and the UTM, along with the corrected values, are illustrated in the Figure 2b, highlighting the differences.

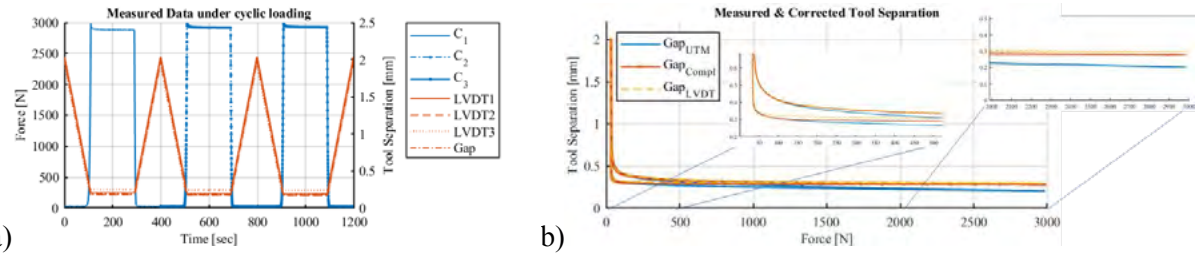

Figure 2. Experimental data; a) Force and tool separation under cyclic loading, b) Measured with UTM, LVDTs and corrected after compliance curves, tool separation.

The thickness and the width of the samples varied depending on the number of rovings for each configuration and the tension levels, and thus the maximum fiber volume fraction achieved during the tests differed. The width was measured using a caliper both before and after each test. Consequently, the fiber volume fraction of each specimen was estimated based on the number of rovings and its cross-sectional area. The following equation (Eq. 1) was employed for the calculation of the fiber volume fraction:

$$V_f = N \cdot \frac{m_l}{\rho \cdot w \cdot t} \tag{1}$$

where N is the number of rovings, m_l is the linear fiber weight equal to 0.8 $^{g}/_{m}$, ρ is the carbon fiber density equal to 1.8 $^{g}/_{cm^3}$, w is the measured width of each specimen and t is the measured tool separation.

3. Results

As previously mentioned, the rovings were unconfined, allowing for movement in the transverse direction, consequently altering their final width due to compression. The average width difference, expressed as a percentage of the initial specimen width, along with the standard deviation for each case study, is presented in Table 1.

Table 1. Average width difference (w_d) in percentage of initial width *(Standard deviation).

Configuration	Tension w_d [%]	T_0	T_1	T_2
C_4		3.53 (0.21)	1.55 (0.40)	1.43 (0.42)

C_9	3.45 (1.23)	1.78 (1.40)	0.64 (0.24)
C_{11}	4.24 (0.53)	1.49 (0.36)	0.57 (0.44)

Table 1 illustrates that alterations in width are less pronounced when higher tension is applied. Transverse dislocation of filaments is limited in the presence of tension, with width alterations likely originating from the compressibility and nesting of rovings. As the maximum width difference corresponds to less than 4.5% (C_{11}-T_0 case) of the initial width for each specimen, it can be assumed that stress values can be estimated using the final measured width. Furthermore, stress was calculated by dividing the force measured by the UTM by the specimen's final surface area.

The average values for each tension and configuration group are presented as follows. Initially, the measured force and tool separation were interpolated over the testing time of each case, ensuring that the averaging corresponds to the same data length. Figure 3 illustrates the average calculated stress for each tension level and configuration over the volume fraction change during the first cycle of the experiments.

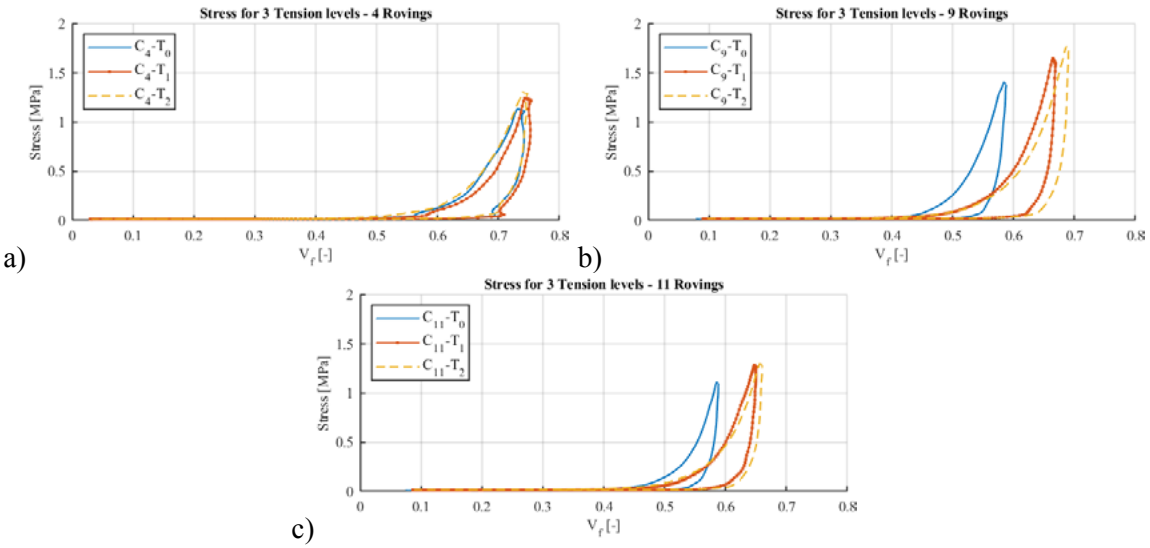

Figure 3. Average measured stress for each tension level over the volume fraction change for the first cycle of the configurations; a) 4 rovings, b) 9 rovings, c) 11 rovings.

It is apparent from the stress curves that the applied tension affects the compressibility of the roving configurations with 9 and 11 rovings. For these configurations, the calculated stress over the volume fraction changes for the two tension levels is very similar, whereas the curve for zero tension deviates significantly from the cases with tension. The variability of the average stress curve for the 4 rovings configuration is higher than the rest cases (Figure 3a). This rovings arrangement was challenging as the thickness of a single row is variable and it was compressed reaching Vf values close to 0.75.

A power-law function which is given in the following equation (Eq. 2) was fitted to the compaction curves using the normalized stress ($\bar{\sigma}$, 1 MPa) as proposed by Robitaille et al [4]. The fitting parameters α, β for each case study and through the first cycle are presented in Table 2. The coefficient of correlation, R^2 between the measurement data and the fit curves for all the reported constants was above 0.99. Data points which correspond to low stress values, meaning that there is no significant contact between the plates and the rovings, were removed to achieve a good fit of the stress curves. The curve fitting of Eq. 2 to the normalized stress over the V_f for all cases during the first cycle of the tests is shown in Figure 4.

$$V_f = a \cdot \bar{\sigma}^{\beta} \quad (2)$$

Table 2. Fitting constants α, β for Eq. 2 in stress curves of the first cycle.

Configuration \ Tension	T_0		T_1		T_2	
	α	β	α	β	α	β
C_4	0.723	0.092	0.733	0.084	0.722	0.101
C_9	0.565	0.093	0.638	0.103	0.652	0.113
C_{11}	0.585	0.086	0.637	0.093	0.645	0.105

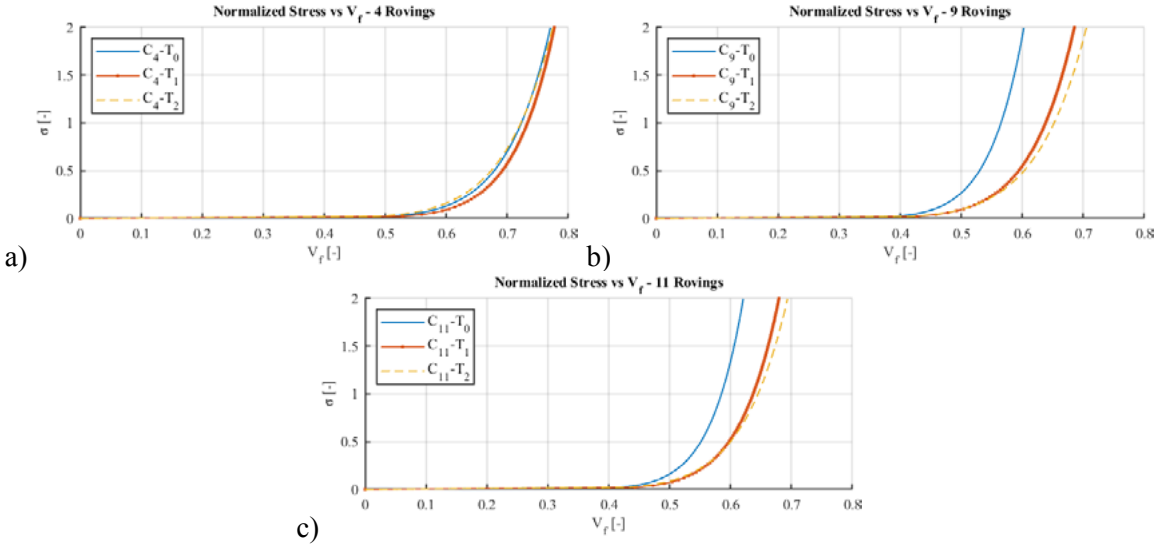

Figure 4. Fit of Equation 2 to the normalized stress data for the first cycle;
a) 4 rovings, b) 9 rovings, c) 11 rovings.

Data were extracted from the experiments contribute to understanding compaction behavior according to the latest benchmark [2]. These data points include: maximum compaction stress, volume fraction (V_f) at maximum stress, V_f at a specific stress level (in this case, 1 MPa), and the stress at the end of the hold time. The arrangement of the case studies using stress and V_f values can provide an indication of the effects of tension and configuration on compressive performance. Some observations regarding extracted data, which are related to the compaction behavior during the first cycle of testing, are presented in Figure 5.

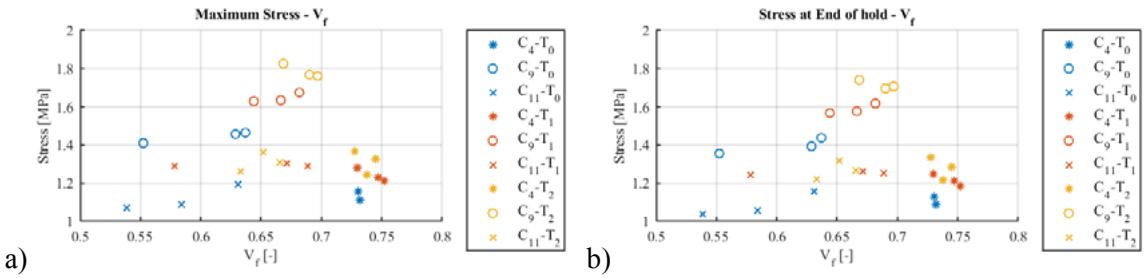

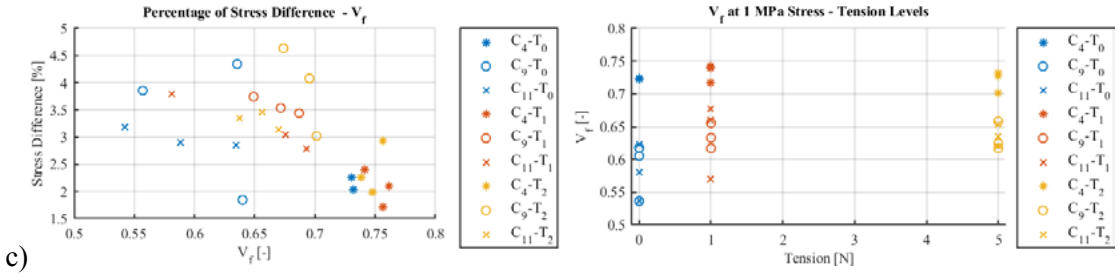

c)

Figure 5. Observations on various roving configurations and tension levels obtained; a) Maximum stress and its corresponding V_f, b) Stress at the end of hold time, c) Percentage difference between maximum and end of hold time stresses, d) Reached V_f values at 1 MPa stress.

It can be seen that in general the variability of the results is higher with the zero tension cases due to the fact that the rovings are unconstrained in the transverse direction. The unconfined geometry allows the free movement and rearrangement of the rovings and in cases of no tension this movement is more dominant. Additionally to the average compaction curves (Figure 3), these results indicate that the applied tension alters the compressive performance of each configuration, resulting in an increase in the maximum achieved stress and V_f for all cases. However, the compressive performance is mostly influenced by the arrangement of the rovings. For example, as shown in Figure 5a and 5b, the highest stress values for all tension levels were observed in the C_9 quadratic case. This can be related to the effective cross-area of rovings contributing to the compressibility which is higher in C9 case than the rest. The stress values at the end of hold time indicate that there is a drop in all cases as it is shown in Figure 5c. Further investigation on the data after each cycle could provide more insights to the relaxation phenomena occurred during the holding period.

4. Conclusions

In this study, the compaction behavior of roving-based reinforcements under various conditions was examined using a new experimental setup. This setup facilitated multiple roving configurations under different tension levels while minimizing friction at their holding locations. The primary focus was to highlight the effects of tension on various roving patterns.

The results presented indicate that tension alters the behavior of roving configurations, allowing for higher compaction with increased tension particularly in cases with a more complex pattern than a single row. Higher tension reduces the lateral movement of rovings resulting to a more oriented alignment, thereby requiring lower compaction force to achieve a desired compaction level. The main contribution to the overall compressibility characteristics originates from the selection of the roving configuration. This information can be particularly useful when designing the continuous processes such as when designing roving guides for pultrusion process.

Future work suggested by this study includes the use of a confined geometry and the investigation of wetted rovings. A confined geometry would eliminate the width measurement uncertainty of the specimens and increase the accuracy of the results. However, the influence of the transverse constrains and the lateral effects due to the applied tension could differ from those observed in this study.

References

[1] P. A. Arrabiyeh, D. May, M. Eckrich, & A. M. Dlugaj. An overview on current manufacturing technologies: Processing continuous rovings impregnated with thermoset resin. *Polymer Composites*, 42(11): 5630-5655, 2021.

[2] A. X. Yong, A. Aktas, D. May, A. Endruweit, S. V. Lomov, S. Advani, ... & J. H. Wang. Experimental characterisation of textile compaction response: A benchmark exercise. *Comp Part A: Applied Science and Manufacturing*, 142:106243, 2021.
[3] Y.R Kim, S.P. McCarthy, & J.P Fanucci. Compressibility and relaxation of fiber reinforcements during composite processing. *Polymer composites*, 12(1): 13-19, 1991.
[4] F. Robitaille, & R. Gauvin. Compaction of textile reinforcements for composites manufacturing. I: Review of experimental results. *Polymer composites*, 19(2): 198-216, 1998.
[5] O. Yuksel, B. Caglar, G. Broggi, V. Michaud, R. Akkerman, I. Baran. Saturated transverse permeability of unidirectional rovings for pultrusion: The effect of microstructural evolution through compaction. *Polymer Composites*, 45(7): 5935-5952, 2024.
[6] G. L. Batch, S. Cumiskey, & C. W. Macosko. Compaction of fiber reinforcements. *Polymer composites*, 23(3): 307-318, 2002.
[7] M. Sandberg, J. H. Hattel, & J. Spangenberg. Flow-Induced Fibre Compaction in Resin-Injection Pultrusion. *Transport in Porous Media*, 147(3): 541-571, 2023.
[8] M. Volk, O. Yuksel, I. Baran, J. H. Hattel, J. Spangenberg, & M. Sandberg. Cost-efficient, automated, and sustainable composite profile manufacture: A review of the state of the art, innovations, and future of pultrusion technologies. *Comp Part B: Engineering*, 246: 110135, 2022.
[9] A. A. Safonov, P. Carlone, & I. Akhatov. Mathematical simulation of pultrusion processes: A review. *Composite Structures*, 184: 153-177, 2018.
[10] TORAY, T700S Rev. 3: Updated January 17, 2018.